Author(s): Saarnio, Ville K.; Salorinne, Kirsi; Ruokolainen, Visa P.; Nilsson, Jesper R.; Tero, Tiia-Riikka; Oikarinen, Sami; Wilhelmsson, L. Marcus; Lahtinen, Tanja M.; Marjomäki, Varpu S.

Title: Development of functionalized SYBR green II related cyanine dyes for viral RNA detection

Year: 2020

Version: Accepted version (Final draft)

Please cite the original version:

Saarnio, V. K., Salorinne, K., Ruokolainen, V. P., Nilsson, J. R., Tero, T.-R., Oikarinen, S., Wilhelmsson, L. M., Lahtinen, T. M., & Marjomäki, V. S. (2020). Development of functionalized SYBR green II related cyanine dyes for viral RNA detection. Dyes and Pigments, 177, Article 108282. https://doi.org/10.1016/j.dyepig.2020.108282

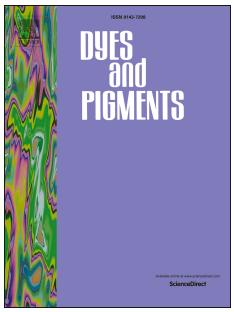

Development of functionalized SYBR green II related cyanine dyes for viral RNA detection

Ville K. Saarnio, Kirsi Salorinne, Visa P. Ruokolainen, Jesper R. Nilsson, Tiia-Riikka Tero, Sami Oikarinen, L. Marcus Wilhelmsson, Tanja M. Lahtinen, Varpu S. Marjomäki

PII: S0143-7208(19)32647-6

DOI: https://doi.org/10.1016/j.dyepig.2020.108282

Reference: DYPI 108282

To appear in: *Dyes and Pigments*

Received Date: 15 November 2019

Revised Date: 17 January 2020

Accepted Date: 13 February 2020

Please cite this article as: Saarnio VK, Salorinne K, Ruokolainen VP, Nilsson JR, Tero T-R, Oikarinen S, Wilhelmsson LM, Lahtinen TM, Marjomäki VS, Development of functionalized SYBR green II related cyanine dyes for viral RNA detection, *Dyes and Pigments* (2020), doi: https://doi.org/10.1016/j.dyepig.2020.108282.

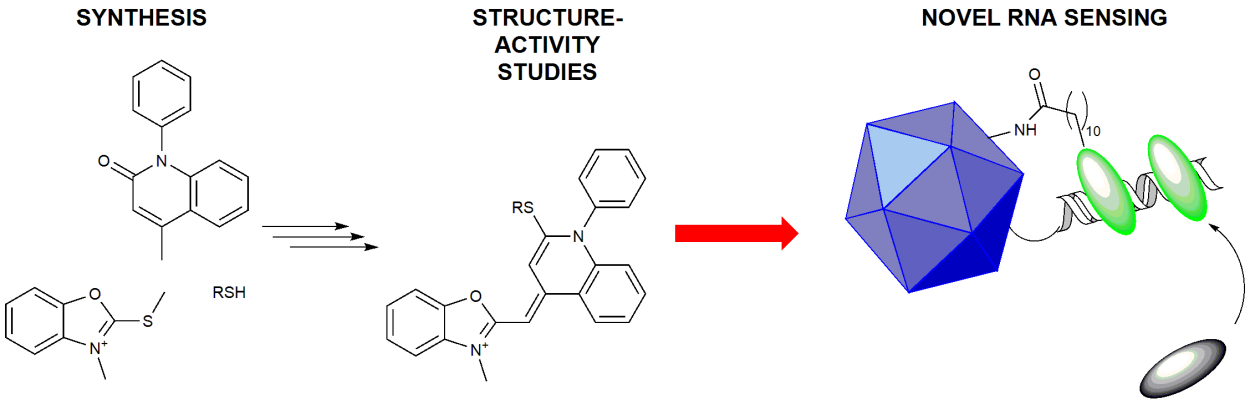

Development of Functionalized SYBR Green II Related Cyanine Dyes For Viral RNA Detection

Ville K. Saarnio, Kirsi Salorinne, Visa P. Ruokolainen, Jesper R. Nilsson, Tiia-Riikka Tero, Sami Oikarinen, L. Marcus Wilhelmsson, Tanja M. Lahtinen*, and Varpu S. Marjomäki*

Abstract: Fluorescent probes for sensing nucleic acids have found widespread use in the field of cell and molecular biology. However, probes combined with potential for post-synthetic conjugation, *e.g.* for intra-endosomal measurements of RNA, are unavailable. Herein we developed cyanine dyes that can be conjugated to viral capsid or other targets. First, we solved the crystal structure of SYBR Green II. The structural elucidation of this commonly used RNA probe provided the basis for synthesizing similar molecules with much desired function for post-synthetic conjugation. To address this need, cyanine dyes were prepared using an alternative synthesis protocol. All studied compounds showed considerable brightness upon binding to nucleic acids. However, regardless of the common chromophore on the dyes, the observed fluorescence emission intensities varied significantly, where methyl-substituted dye **1** gave values higher than SYBR Green II, whereas compounds **2**-**5** containing undecyl spacers had lower values. Studying the structure-activity relationship revealed the longer alkyl chains to induce slight perturbation in dye intercalation, as well as demanding larger binding area on the nucleic acid lattice, explaining these differences. To study the potential biological use of the dyes, the RNA genome of enterovirus echovirus 1 was studied *in vitro* with the probes. A novel method employing the low binding space requirement of **1** was developed to determine the single-to-double-stranded RNA ratio of a sample, whereas compound **4** was covalently bound to the viral capsid and used successfully to monitor the viral RNA release from within the capsid. The presented results open new possibilities for preparation and use of SYBR Green-based nucleic acid probes to further apply these compounds for increasingly demanding targeting in biological contexts.

1. Introduction

Many fluorescent probes for sensing nucleic acids are available nowadays. However, targeting possibilities for excluding interfering background signal from the molecules of interest remain suboptimal. For example, tools for sensing viral RNA from the background DNA/RNA present in a cellular environment are lacking. For such detection, a combination of light-up upon target binding and control over localization is desired. Cyanine dyes are defined as an organic molecule containing two nitrogen substituted heterocycles sharing a cationic charge through a polymethine bridge [1]. They are usually prepared with classical cyanine condensation reactions between two quaternary amine salts. [2] Among their widespread applications, one of particular interest is their use as fluorescent probes [3]. For example, the Cy-family of symmetrical cyanine dyes is widely employed in different biological applications [4]. Most of these compounds have molar absorptivities in the magnitude of 10^4 – 10^5 $cm^{-1}M^{-1}$, with different compounds covering the whole visible light spectrum [2]. However, arguably the most important application of these compounds as fluorophores has been the use of unsymmetrical dyes for detection of nucleic acids through noncovalent binding, exhibiting an up to 1000-fold increase in fluorescence intensity upon binding [1]. A well-studied example from such dyes exhibiting this behavior is the thiazole orange (TO), consisting of monomethine bridged benzothiazolium and quinolinium units. [5] TO together with oxazole yellow (YO) and their homodimers (TOTO and YOYO) have served as a foundation for continuous development of these dyes [6–10]. The research on these dyes has also led to a wide range of commercially available nucleic acid stains [11]. Important and widely used commercial fluorophores include SYBR Green I, SYBR Green II, SYBR Safe, SYBR Gold and PicoGreen. While the chemical structures of PicoGreen [12], SYBR Safe [13] and SYBR Green I [12] have been reported, many routinely used compounds are still unknown [11]. A common descriptor for these dyes is their ability to interact with DNA and RNA, by intercalation [14].

Intercalators bind to double-stranded nucleic acids by assuming a planar conformation and inserting between stacked basepairs, forming π-π interactions with the target [14]. The reason for the great fluorescence enhancement is thought to be the result of restriction of the torsional motion of the molecule [15]. The group of Geddes [16,17], has shown that both PicoGreen and SYBR Green I form a similar complex with dsDNA, in which the aromatic quinolinium core unit intercalates into the dsDNA, while the benzothiazolium unit, carrying a localized positive charge enhances the binding affinity by providing additional electrostatic interactions with the DNA backbone. In addition, the dimethylaminopropyl side chains are positioned in the minor groove of the DNA for added stability of the complex [16,17]. However, knowledge on this family of dyes is mostly based on very few examples. Thus, understanding the structural and binding properties of the dye molecules is highly important when studying their binding and interaction with RNA or DNA. It is also crucial for future development of more selective, efficient and versatile dyes that enable the study of more complex biological systems, such as viruses and their mode of action in living cells.

[*] V. K. Saarnio, Dr. K. Salorinne, Dr. T.-R. Tero, Dr. T. M. Lahtinen*
Department of Chemistry, Nanoscience Center,

V. P. Ruokolainen, Dr. V. S. Marjomäki*
Department of Cell and Molecular Biology, Nanoscience Center
University of Jyväskylä
Jyväskylä, FI-40500, Finland
E-mail: tanja.m.lahtinen@jyu.fi
varpu.s.marjomaki@jyu.fi

[b] Dr. J. R. Nilsson, Prof. L. M. Wilhelmsson
Department of Chemistry and Chemical Engineering, Chemistry and Biochemistry
Chalmers University of Technology
Gothenburg, SE-41296, Sweden

[c] Dr. S. Oikarinen
Faculty of Medicine and Life Sciences
University of Tampere
Tampere, FI-33014, Finland

The development of cyanine dyes for selective binding to nucleic acids has enabled the quantification of RNA or DNA content in various biological samples, and inspired their use as fluorescent probes in cell and molecular biology [18]. Nowadays, visualization of nucleic acids in electrophoresis gels using such dyes is performed routinely in cell and molecular biology laboratories [19]. Additionally, recent developments have enabled increasingly selective detection of different base content or secondary structure of nucleic acids [20,21]. However, imaging of larger macromolecular assemblies containing nucleic acids, such as RNA-containing viruses upon internalization into cells, is more challenging due to lower number of viruses in endosomes against a high background of messenger and transfer RNA in the cytoplasm. In addition, dynamic imaging of virus opening in cellular vesicles, a key step during infection, is problematic due to difficulties in targeting the dye to the same structures exclusively. The presently available dyes such as SYBR Green II are hydrophobic and easily cross all cellular membranes thus labeling all RNA in the cell. For successful imaging of *e.g.* virus particles in endosomes, one needs to have a nucleic acid detecting dye which can be conjugated to the virus or a suitable solid support to be endocytosed to the same structures, and not leaking to the cytoplasm. In addition, an optimal dye should also be highly specific for nucleic acids over other contaminating background material, sufficiently high in brightness for imaging by microscopy techniques, and low in cytotoxicity when working with living cells.

The aim of this work was to create cyanine dyes that can be covalently bound to the target material, such as virus capsids or nanoparticles for targeted RNA detection in microscopy imaging. As a basis for this, we used the widely employed RNA probe SYBR Green II after resolving its previously unknown chemical structure. Hence, the dyes synthesized in this work are all 2-thiol substituted and carry an oxazole moiety. A new synthetic pathway to produce similar such dyes was developed and five new compounds (**1**-**5**) were made. The rationale behind the use of a longer 11 carbon chain was to minimalize steric hindrance after conjugation. Spectroscopic evaluation of these dyes gave plausible explanations to the differences in brightness and revealed new information on the structural-activity relationships of these types of compounds. As a proof of principal, two of the most promising compounds **1** and **4** were applied in our case study, to probe the RNA genome of echovirus 1 (EV1), in novel ways impossible to implement with SYBR Green II.

2. Results and Discussion

2.1. Synthesis and Structural Properties

The synthetic pathway designed and used to produce molecules is presented in Scheme 1. First the 2-quinolone **6** was chlorinated using phosphorus oxychloride [22] in order to produce chloroiminium ion **7**. To avoid any undesired side reactions with the thiols, the solvents were evaporated before the next step. For the nucleophilic substitution of the chlorine, the thiol was added together with triethylamine and mixed for 4-6 days at room temperature in dry dichloromethane. After this, the cyanine condensation was carried out as described by Karlsson *et al.* in order to obtain the desired products [8]. Despite the efforts made to avoid reactions with the methyl thiolate, compound **1** was obtained as a side product from each synthesis due to the active thiolate from benzoxazole **9**. The intermediates and products were separated with flash column chromatography and gave MeS **1** with 10 % – 15 % and the other dyes with 10 % – 37 % yields. Individual yields and synthetic details are presented in the SI. From compound **3** the NHS-ester **4** was synthesized together with N-hydroxysuccinimide (NHS) using Steglich esterification [23]. As the carboxylic acid moiety **3** proved very difficult to work with due to apparent impurities in the product, the methyl ester **5** was produced in an identical manner using methanol instead of NHS.

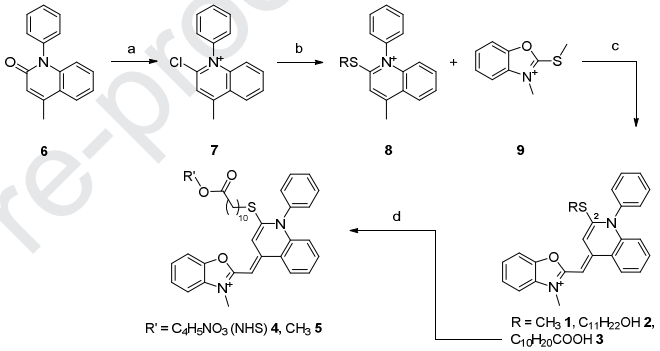

Scheme 1. Synthesis scheme for SYBR Green II related compounds. Reagents: a) $POCl_3$, 1,2-DCE, Δ; b) HSR (R = $C_{11}H_{22}OH$, $C_{10}H_{20}COOH$), Et_3N, DCM c) Et_3N, DCM d) DCC, DMAP and methanol or N-hydroxysuccinimide.

The presented synthesis procedure is straightforward, giving 2-thiol substituted cyanine dyes in three steps. Although a limited number of derivatives were made, the synthesis should be applicable with any other thiol, provided the compound is not sensitive to the basic conditions of the cyanine condensation. The yields of desired products could be improved by for example employing a stronger base in the nucleophilic substitution step to further promote thiolate formation. The substitution of the leaving group could be used as an advantage by manipulating the benzoxazole **9** to already contain the desired arm moiety. The structures of the synthesized dyes and the commercial ones used as comparison are presented in Figure 1.

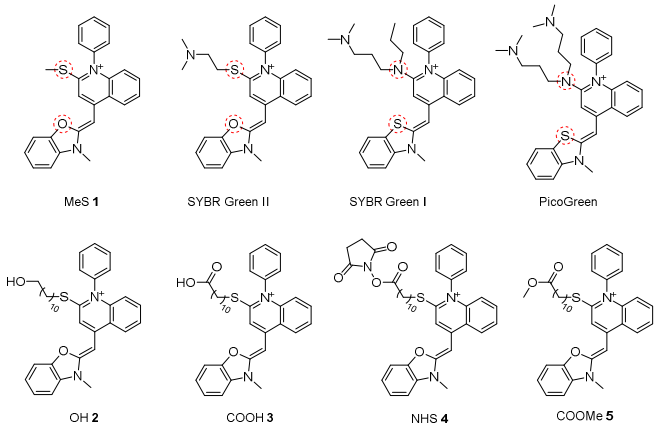

Figure 1. Structures of the synthesized dyes (**1**-**5**). The structures of SYBR Green I, SYBR Green II and PicoGreen are shown for reference. The structural differences on the chromophores of the commercial dyes and MeS **1** are highlighted.

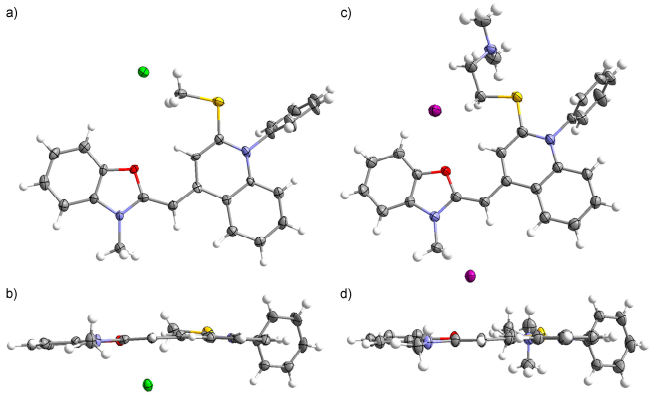

Figure 2. Ortep drawing at 50 % probability level of the crystal structure of MeS dye **1** shown from a) top and b) side views, and of SYBR Green II shown from c) top and d) side views. Element colors: carbon = grey, hydrogen = white, oxygen = red, nitrogen = blue, sulfur = yellow, chlorine = green and iodine = purple.

While the structures of SYBR Green I and PicoGreen are known from literature, the structure of SYBR Green II was here elucidated through X-ray crystallography, together with MeS **1** (Figure 2a, b). The only difference in structure between the MeS dye **1** and SYBR Green II is the different pendant arm on the molecule. Comparing the crystal structure of SYBR Green II (Figure 2c, d) to SYBR Green I and PicoGreen, the thiazole moiety is replaced with an oxazole and the 2-substituent is a thiol instead of a tertiary amine. As a result, SYBR Green I and PicoGreen have two propyl chains attached to the chromophore whereas SYBR Green II only has a 2-(dimethylamino)-ethyl group as the single “arm” on the molecule. The crystallographic details of the two compounds are summarized in Table S1-S3. Dyes **2**-**5** did not crystallize in similar conditions, presumably due to the long alkyl chains hindering the crystal lattice formation. The functional group of the pendant arm affects the charge of the molecule. At slightly acidic pH, the *N*-2-(dimethylamino)-ethylthiolate arm of SYBR Green II can take on an additional positive charge by protonation of the amino group. This significantly improves the water solubility of the dye in comparison to the MeS dye **1**, as observed in the UV-vis measurements presented below.

2.2. Chromophore and Binding Properties

The structure of the chromophore unit of SYBR Green I related compounds is known from literature, and we discovered the structure of SYBR Green II to differ only by two hetero atoms (Figure 1). These minor structural differences lead to a hypsochromic shift in the absorption of SYBR Green II compared to SYBR Green I, as shown in Figure 3. The novel dyes presented in this work display absorption spectra that are similar to each other and to that of SYBR Green II. The differences in spectral characteristics can thus be attributed to the differences in the indoline (S *vs.* O) and the arm-binding hetero atom (N *vs.* S) shown with red circles in Figure 1. Given the structural similarity, it would be expected that these molecules have molar absorptivities similar to that of SYBR Green II. Initial attempts to determine the molar absorptivity for the synthesized molecules (**1**-**5**) in TE buffer did, however, result in significantly different values for each dye. This is explained by the formation of aggregates (most likely H-type) and was particularly notable for the dyes aimed for biofunctionalization (**2**-**5**), as evidenced by scattering and hypsochromically shifted shoulders in the absorption spectra caused by H-aggregates (see Figures S8-S12). The problem of aggregation was circumvented by changing the solvent to DCM (Table 1).

Table 1. Molar absorptivity measured in TE buffer and DCM at their lowest energy absorption maxima (*ca.* 478 nm) derived from Figures S26 and S27.

Solvent	MeS **1**	OH **2**	NHS **4**	COOMe **5**	
TE buffer	19.2 ± 0.6	22.0 ± 0.5	18.5 ± 0.2	7.9 ± 0.5	$\times 10^3$ cm^{-1} mol^{-1}
Dichloromethane	31.1 ± 0.3	38.8 ± 0.5	30.3 ± 0.9	11.6 ± 0.4	

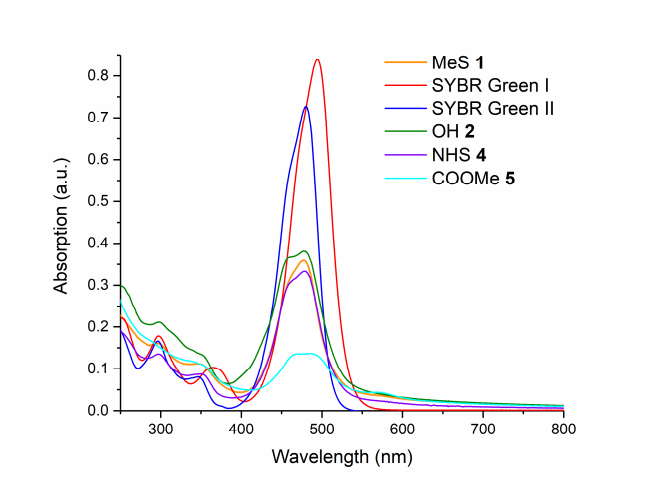

Figure 3. UV-vis spectrum of MeS **1**, OH **2**, NHS **4** and COOMe **5** measured in TE Buffer at 19.6 µM concentration together with SYBR Green I and SYBR Green II at 1:1000 dilution from their respective stock solutions.

While the absorption characteristics of different dyes greatly impact their brightness, it is equally important to evaluate the binding properties of said dyes. One way to gain insight on the orientation of molecules in a ligand-substrate interaction is to employ flow-oriented linear dichroism (LD). A short introduction to the method is presented in the SI page 7. To determine the binding mode to double-stranded DNA and investigate if the attachment of an alkyl-linker to the ligands affects the binding characteristics, LD was measured on the synthesized dyes. The alkyl-containing compounds, MeS **1**, OH **2**, NHS **4**, and COOMe **5** (see Figure 1 for structures) were included in the LD-analysis. LD^r at 260 nm for a sample containing only DNA (θ = 90° for DNA bases in B-form duplex) was used to determine the orientation factor (found to be $S = 0.017$, Figure 4). When studying the samples containing both DNA and ligand, using identical shear flow orientation conditions as for only DNA, a distinct negative LD band corresponding to the lowest energy electronic transition (centered at 484 nm, Figure 4, middle panel) was observed for MeS **1**, OH **2**, and NHS **4**. For COOMe **5**, only a very weak overall LD signal was observed, also appearing as a negative band in the 480 nm region (data not shown). The weak LD signal for **5** is likely caused by poor compound solubility and aggregation in the aqueous solution, as evidenced by significant scattering in the isotropic absorption, hampering the evaluation of COOMe **5** under these experimental conditions. For MeS **1**, OH **2**, and NHS **4** LD^r at 484 nm, where the dye is the sole chromophore (with a transition dipole moment assumed to be in the plane of the essentially coplanar benzoxazolium and quinolinium heterocycles), was used to evaluate the binding angles relative to the DNA long axis. These were determined to be 86°, 70°, and 69° for MeS **1**, OH **2**, and NHS **4**, respectively. The calculated binding angles, in combination with the exclusively negative LD spectra, suggest DNA-binding by intercalation for the three analyzed compounds. It is noteworthy that OH **2** and NHS **4** (both having the alkyl linker) exhibit similar binding angles, yet lower than that of MeS **1**. This suggests that the binding mode of OH **2** and NHS **4** to DNA, although of evident intercalation character, is slightly affected by the presence of the attached linkers. From the differences in binding angles it is conceivable that the linker participates in the binding by associating to one of the grooves of the DNA duplex, causing a slight displacement (tilt) of the ligand between the stacked bases and possibly also a slight distortion from exact coplanarity of the benzoxazolium and quinolinium moieties. This notion of a slight change in binding mode is further supported by the observed differences in binding constants and binding site size as described below. Understanding the impact the linking arms have on the nucleic acid binding modes of these dyes, before putting them into use in biological applications, is imperative.

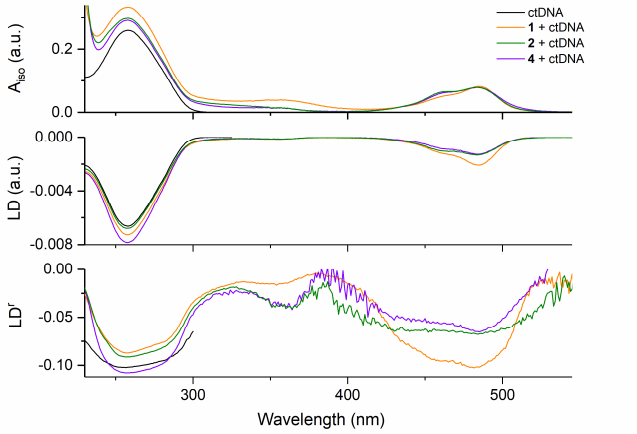

Figure 4. Absorption and LD spectra of DNA in TE buffer with and without ligand. Concentration of DNA and ligand (where present) were 100 µM and 0.5 µM, respectively. DNA only (black line), DNA + MeS **1** (orange line), DNA + NHS **4** (violet line) and DNA + OH **2** (olive line). Top panel: Isotropic absorption. Middle panel: Linear dichroism. Bottom panel: Reduced linear dichroism (LD^r). Note that the difference in optical path length of the LD Couette cell (1 mm) and the cuvette used to determine A_{iso} (4 mm) was considered when calculating LD^r, *i.e.* $LD^r = 4 \times LD/A_{iso}$.

For all synthesized compounds and SYBR Green II, the emission maximum wavelength was very close to 505 nm (Figure 5), leading to compounds containing similar Stokes shifts in comparison to SYBR Green I. The emission maxima, when bound to fully double-stranded DNA remain the same, but as the portion of single-stranded nucleic acid is enhanced, increasing bathochromic shifts are also observed. This was observed as a small bathochromic shift to 515 nm when binding to cellular RNA (rRNA), while the fully linear 50 base ssDNA (liDNA) exhibits a significant shift to *ca.* 560 nm, as shown in Figures S13-S18. Similar to the commercial dyes, the fluorescence of the synthesized dyes in solution without DNA was negligible, presumably due to non-radiative relaxation pathways (such as the rotation of the N-phenyl ring). Upon intercalation the fluorescence increases over a thousand-fold with SYBR Green I and similar enhancements are observed with the dyes prepared here (**1**-**5**). It is evident that higher intensity of emission was obtained for MeS **1** compared to SYBR Green II for all four types of nucleic acids used (see Figures 6, S19, S20, and S22). These

nucleic acids included rRNA, calf thymus DNA (ctDNA), bacterial double-stranded plasmid DNA (λDNA), liDNA and self-pairing hairpin forming 50 base ssDNA (hpDNA). SYBR Green I emits most strongly, but noticeably as the binding DNA gets more sterically demanding, the intensity difference compared to MeS dye **1** starts to diminish. This is clearly observed when moving from fully double-stranded DNA to rRNA, but the difference between SYBR Green I and MeS **1** gets significantly lower, when moving from ctDNA to hpDNA. The emission spectra of the dyes upon binding to liDNA (Figures S13-S18, and S21) shows a large bathochromic shift compared to binding to the other nucleic acids but the intensity of this fluorescence remains small. The dyes containing longer 2-substituents seem to exhibit this characteristic more strongly, possibly indicating a different type of binding mode than intercalation that contributes to the lower energy emission. This suggestion is further supported by the divergence in intercalation angle observed for dyes **2** and **4** in the LD experiments. The emission intensities of thiol-substituted dyes stay proportional between each other with the different nucleic acids, whereas SYBR Green I experiences dramatic loss in emission when it is measured with nucleic acids that are not fully double-stranded. The fluorescence intensities of the long alkyl chain-containing dyes **2**, **4**, and **5** are significantly lower compared to the MeS dye **1**, yet still sufficiently bright to be applicable for the biological systems of interest here. In order to better understand the dye-nucleic acid interactions that lead to these differences in emission intensities with probes containing the same aromatic unit, a detailed analysis of fluorescence titration data was conducted, presented below.

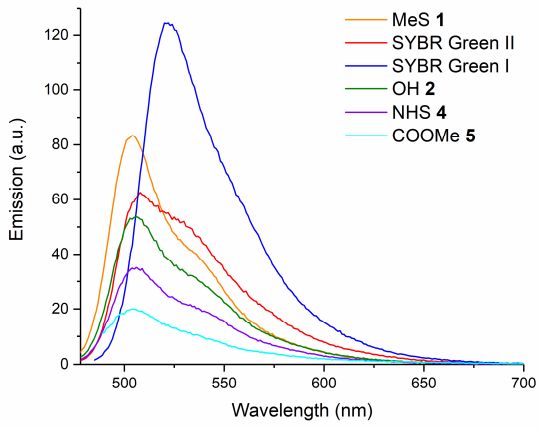

Figure 5. Fluorescence spectra of the tested cyanine dyes measured in TE buffer with 0.52 µM ctDNA at 21 °C. A 1:200 000 dilution from each stock was made corresponding 0.1 µM concentration except for COOMe **5** 1.0 µM was used.

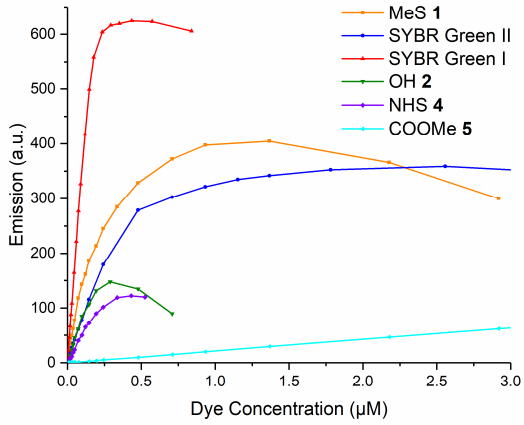

Figure 6. Binding isotherms from titrations of different dyes in 0.52 µM ctDNA in TE buffer at 21 °C.

Titration experiments conducted at pH 7.6 with each of the nucleic acids and plotting the highest values of emission intensity as the concentration increases gave binding isotherms for the interaction with dsDNA, displayed in Figure 6 for ctDNA and Figures S19-S22 for the other nucleic acids studied here. From this data it is possible to determine the binding constant to double-stranded DNA according to the methods employed by Dragan *et al*. for SYBR Green I [17] and PicoGreen [16]. In short, the theoretical expression for DNA-ligand interactions, McGhee von Hippel equation [24] for non-cooperative binding of ligands can be used to gain deeper insight into interactions between dyes and double-stranded nucleic acids:

$$v/L = K_a(1-nv)^n / (1-nv+v)^{n-1} \quad (1)$$

where v is binding density of ligands in DNA, L is unbound ligands, K_a is the binding constant for complex formation and n is the size of the binding site of ligand in base pairs. The formation of supramolecular complex between the dye and dsDNA is an equilibrium reaction as shown in equation 2:

$$\text{Dye} + \text{dsDNA} \rightleftarrows [\text{Dye:dsDNA}] \quad (2)$$

that can be described with the McGhee and Von Hippel equation [24]. From the binding isotherms, it is possible to express the fraction of dye molecules bound to DNA (θ) with the fraction of fluorescence observed (F) compared to fluorescence from 100 % binding (F_b) as shown in equation 3:

$$\theta \approx F/F_b. \quad (3)$$

The F_b was obtained from titration of dyes to high excess of DNA and the resulting linear behavior (Figure S23). Equation 3 ignores the effect of non-bound dye to the fluorescence, which is reasonable as its contribution is negligible in all cases presented here.

Using θ it is possible to determine the concentration of free molecules in solution (L) according to equation 4

$$L = (1 - \theta)c \quad (4)$$

and binding density (v) of bound dye molecules

$$v = \theta c / c_{DNA}\,, \quad (5)$$

where c is the concentration of the dye and c_{DNA} is the concentration of the nucleic acid in solution. Processing the generated data according to equations 3-5 gives the Scatchard plots shown in Figure 7, S24 and S25, where a fit to equation 1 was done in order to get the binding constant and the binding site size for individual dye molecules expressed in base pairs. The data for ctDNA from this procedure is summarized in Table 2.

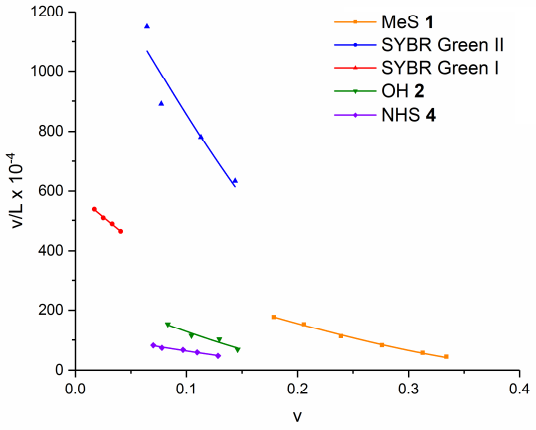

Figure 7. Scatchard plot for cyanine dyes binding to ctDNA based on the data from Figure 6 and S23 and fitting based on McGhee von Hippel equation 1.

Table 2. Summarized ctDNA binding parameters attained from fluorescence spectroscopy titrations. Fluorescence quantum yields were derived from Figure S28.

Dye	Binding constant K_a (10^6 M^{-1})	Binding site size n (bp)	Gibbs free energy ΔG (kJ/mol)	Fluorescence quantum yield Φ
MeS **1**	3.9 ± 0.1	2.2 ± 0.03	-37	0.60
SYBR Green II	15 ± 2	2.8 ± 0.5	-40	0.36 [25]
SYBR Green I	5.9 ± 0.05	3.2 ± 0.11	-38	0.80 [26]
OH **2**	2.8 ± 0.4	3.4 ± 0.3	-36	0.47
NHS **4**	1.3 ± 0.06	3.2 ± 0.15	-34	0.63

The binding affinity seems to increase as the arm moiety on the molecules gets longer, suggesting a positive effect of hydrophobic interactions between the nucleic acid groove and the dye arm in binding with λDNA (Table S4). However, as can be seen in Figure 8, this also causes an increase in the size demanded by an individual molecule. The fit done on known values for different dyes indicates a linear dependence between binding site size and the arm length. The outlier in the series, OH **2** is the only molecule with an extended, completely linear 2-substituent and because of this, might be able to insert more completely to the dsDNA lattice. The results of binding site size acquired from ctDNA and λDNA are highly similar for the dyes with shorter "arm" lengths, but discrepancies appear for OH **2** and NHS **4**. Reasons for the better accommodation of long-armed dyes with λDNA could be better uniformity and more continuous dsDNA lattice, whereas ctDNA constitutes of a size distribution of dsDNA oligomers (and ssDNA as a side product). The effect is even more pronounced with hpDNA (Table S4), where unrealistic results are acquired because the theory does not account for the finite length of the dsDNA.

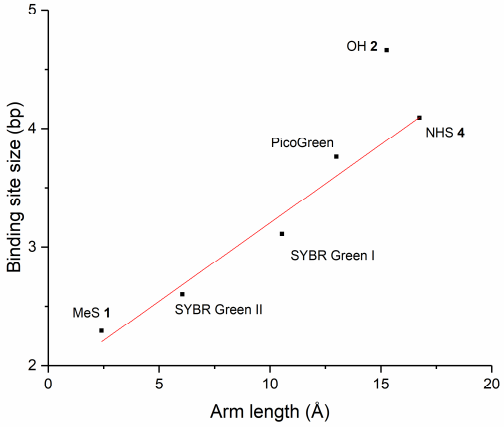

Figure 8. Relationship between the length of the arm moiety on a molecule and corresponding binding site size in binding to λDNA (Table S4).

The positively charged dimethyl amine groups seem to contribute positively to the binding affinity, as evidenced by significantly higher association constants for SYBR Green I and SYBR Green II. The hydroxyl (OH **2**) and carboxylic acid (COOH **3** and COOMe **5**) groups on the other hand carry a negative partial charge, which could affect the groove binding negatively. An indication of this was given by the lower binding affinity of OH **2** compared to SYBR Green I despite its longer arm moiety, but a clear relationship cannot be established. The carboxylic acid functionalized dye **3** posed significant problems considering the sample purity and heavy aggregation in solution and hence the titration experiments were not successful. The fluorescence of the COOMe-functionalized compound **5** varied linearly with concentration throughout the titration, making determination of the binding constants impossible in the attempted concentration regime. The highest obtained fluorescence intensities for each dye with each nucleic acid are presented in Figure 9.

The fluorescence quantum yield for MeS dye **1** when bound to ctDNA is 60 %, which is comparable to the value of 54 % given for SYBR Green II with RNA [25]. The corresponding value for SYBR Green II when bound to ctDNA is 36 %. SYBR Green I, on the other hand, shows a higher quantum yield of 80 % when bound to ctDNA and combined with its higher molar absorptivity, meaning that the thiazole chromophore with a N-linked arm moiety is brighter of the two [26]. The reason for the lower fluorescence saturation of SYBR Green I with rRNA compared to MeS **1** is most likely due to limitations in the number of binding sites available, as each molecule requires a longer stretch of double-stranded nucleic acid for binding. For SYBR Green II, the difference in fluorescence saturation intensity with rRNA may be a result of different binding site size, as the chromophores are the same in both molecules. Thus, the quality of a nucleic acid binding fluorophore is determined by two factors. First, the brightness of the bound chromophore plays a crucial role but, equally important are the parameters affiliated with the binding. With a longer arm on the molecule, the strength of binding increases but in turn so does the size of the binding site. However, packing the probes too tightly on the double-stranded nucleic acids leads to homo-quenching between dye molecules. This means a careful balance exists between maximizing the number of probes bound to a nucleic acid without inducing such proximity between individual probes that leads to quenching. With this information, rational design can be used to synthesize probes that bind to nucleic acids with high affinity, such as SYBR Green I, or probes with slightly lower affinity but higher brightness as an effect of increased number of molecules bound to the target at maximum load, such as MeS **1**.

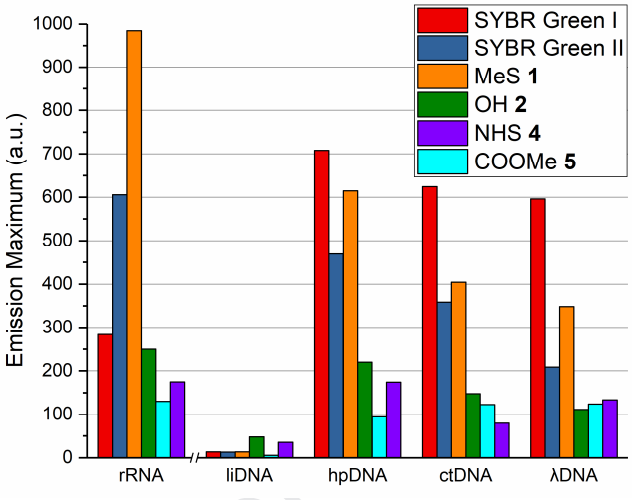

Figure 9. Highest fluorescence values achieved from titrations with different nucleic acids. All the DNA samples were measured using the same settings on the spectrophotometer. All samples were measured in constant nucleic acid concentration in TE buffer at 21 °C and aliquots of respective dye were added until highest value of emission was reached. rRNA = cellular RNA, liDNA = 50 base linear ssDNA, hpDNA = 50 base self-pairing DNA, ctDNA = calf thymus DNA and λDNA = bacterial GLP-GPI plasmid DNA.

As the structures show, the differences between SYBR Green I and SYBR Green II are found in the different hetero atom on the 2-quinoline and 3-indole positions together with the linking arm of the molecules. Surprisingly, for our synthesized dyes, this leads to a significant decrease in the brightness of the chromophore, with the molar absorptivity decreasing by almost a half and the fluorescence quantum yield by 10 % – 20 % compared to SYBR Green I. For the molecules synthesized in this work, this leads to a brightness that is ~40 % of that of SYBR Green I. Although the chromophore of SYBR Green I has a higher brightness in nucleic acid contexts, the emission intensity of SYBR Green II is higher, when binding to rRNA. Importantly, compound **1** reaches even higher intensity when associating to rRNA. This can be explained by the characteristics of the complex formation across different dyes and especially the sizes of the binding site, (*n*) as shown in Table 2. While a single molecule of SYBR Green I occupies (in average) 3.1 base pairs on the dsDNA lattice, the length of lattice required by SYBR Green II and MeS dye **1** is only 2.8 and 2.2 base pairs, respectively. With lower available binding sites for the dyes, MeS **1** is the better nucleic acid probe as it makes better use of the limited binding sites. As proposed by the group of Geddes [16,17] the higher binding affinity comes as an effect of the arm moiety as the alkyl chains settle along the groove. This is something that we also observed here from the high binding constant value of compounds **2** and **4** with λDNA. Additionally, the cationic charge of the dimethylamine group in the arm of SYBR Green I and SYBR Green II adds an electrostatic component to the interaction and also increases the water solubility of the dyes. The synthesized products carry only one positive charge, which is insufficient for solubilizing the

compounds and thus results in aggregation in aqueous solutions, as observed by scattering and aggregation in UV-vis absorption. This should be taken into account in future work by either replacing the arm with a more hydrophilic molecule, such as ethyl glycol, or increasing the charge of the chromophore. Despite the drawbacks in solubility and increased binding site size, the biofunctionalized dyes **2** and **4** are still potent fluorophores. To show this, we evaluated the use of MeS **1** and NHS **4** in *in vitro* experiments on a viral genomic sample, Echovirus 1 RNA, as shown in the following section.

2.3. Case Study: Echovirus 1 Genomic RNA

Viral RNA, as well as cellular RNA, typically forms secondary structures, which is the basis of fluorescence emission upon binding of the dyes synthesized in this work. Presently, there are very few RNA/DNA detecting molecules that could be used to detect viral genome release in cellular vesicles. Therefore, in this study, we aimed at developing RNA binding dyes that can be targeted to cellular vesicles by conjugating to carrier materials that are internalized to vesicles.

In order to prove that MeS **1** is able to detect viral RNA, we first tested the compound with a conventional method to detect RNA released from enterovirus echovirus 1 particles, namely a PaSTRy assay [27]. In this method, the viral genome is released from its capsid by gradually increasing the temperature to 90 °C. Melting temperature is measured to describe the stability of the virus and, for example, to test if drugs stabilize or destabilize the viruses. In the melting curve of virus particles, upon opening of the virus the emission values rapidly rose until about 60 °C, due to the release of viral RNA followed from capsid opening, after which the emission values then started to decrease again, as the rising temperature dissociates the dye-nucleic acid complex (Figure 10). In the measurement, the emission of MeS **1** was significantly higher compared to that of SYBR Green II. This result further supports the observation that MeS **1** provides higher emission intensities compared to SYBR Green II (with sufficiently adjusted concentration). While the improvement in fluorescence intensity with MeS **1** in comparison to SYBR Green II was highly desirable, our initial objective was to develop a similar dye with potential for covalent attachment. To examine the potential of using NHS **4** as such a probe to sense RNA release from the virus capsid, the dye was conjugated to the free lysine residues found on EV1 capsid (see SI for details). NHS **4** conjugated on the echovirus 1 capsid surface gave an observable fluorescence peak (Figure 10), despite being only a fraction in intensity compared to MeS **1**. Such a result was expected because less molecules are present on the capsid surface compared to dye **1** that is free in solution. However, the long alkyl chain on **4** might contribute to weaker binding in higher temperature as well.

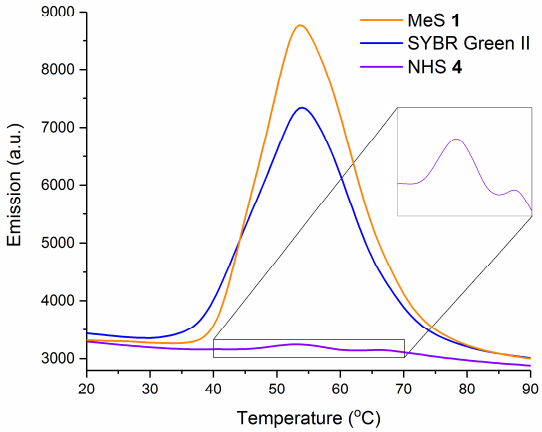

Figure 10. Thermal assay melting curve of EV1 monitored with SYBR Green II, MeS **1**, as well as NHS **4**-conjugated virus particles. Inset: Magnification of the emission trace of **4**.

Next, we tested how our compounds detect viral RNA at physiological temperature in a real-time assay that was previously established in our laboratory [28]. Virus, nucleic acid probes and salt solution, that forces opening of the virus particles, were mixed together at 37 °C and fluorescence emission was followed for 3 hours in a 96-well plate setup in a spectrofluorometer (Figure 11). The results showed that the MeS **1** emission increased within 30 min to high values, due to addition of the opening buffer. Similarly, we tested NHS **4** which was directly conjugated to the virus capsid, thus being very close to the RNA in the event of RNA release. NHS **4** conjugated to the virus understandably showed much lower intensities but still detected virus opening at 37 °C. Thus, the two newly synthesized dyes MeS **1** and NHS **4** demonstrated their usability in nucleic acid sensing. While MeS **1** gave a good signal in the experiment, the values of NHS **4** conjugated on the viral particle surface were only 20 % that of the former (Figure 11). This was an expected result, as the amount of dye **4** molecules bound on the viral capsid surface is significantly lower compared to concentration of MeS **1** in solution. Interestingly, at around 20 minutes the emission of NHS **4** peaked in fluorescence before plateauing to 80 % of the peak emission intensity, possibly indicating the moment where majority of the viral RNA is released from the viral particles before diffusing to the total sample volume. While the emission intensity of NHS **4** is lower *in vitro* compared to MeS **1**, it should be noted that the conjugation to the viral capsid means the emission is better localized.

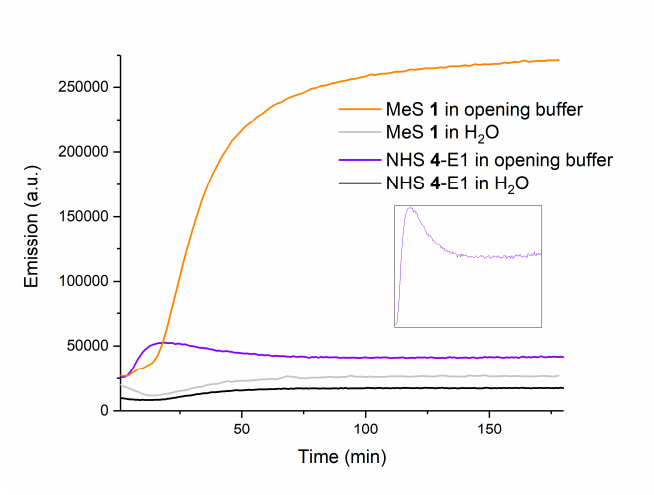

Figure 11. Emission of MeS **1** and NHS **4**-conjugated EV1 capsid in water and buffer solution (20 mM NaCl, 6mM KH_2PO_4, 12 mM K_2HPO_4, pH ~7.2) promoting capsid opening for the EV1 at 37 °C. Inset: Magnification of the Y-axis to display NHS **4** curve better.

As MeS **1** binding was based on binding to double stranded nucleic acid, we next tested whether we could quantify the portion of RNA that is in double-stranded conformation. Previously, many calculation-based estimations about secondary structures in viral RNA genomes have been made [29,30], but to our best knowledge no empirical studies on the degree of RNA duplex in the viral context have been made before. A method monitor the single-to-double-stranded RNA ratio in solution using PicoGreen has been previously reported [31,32]. However, our method aimed to utilize total fluorescence intensity instead of specific wavelengths or fluorescence lifetimes as the variable.

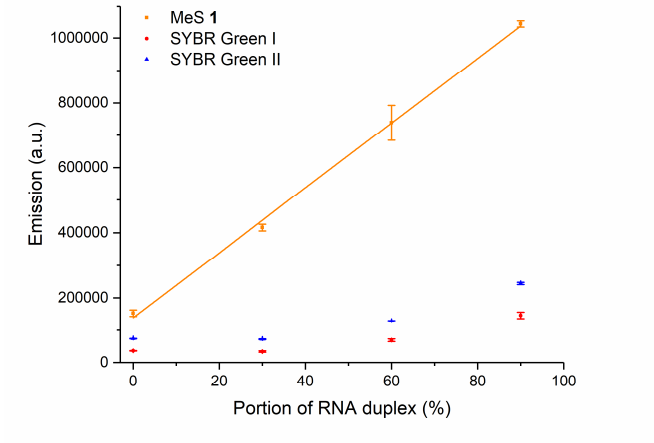

Figure 12. The MeS **1**, SYBR Green I, and SYBR Green II mixed with RNA constructs having varying amounts of double-strand. A 50-mer ssRNA was mixed with equimolar amounts of complementary ssRNA with lengths 15, 30, and 45 bases, respectively. Also shown is a linear fit for compound **1**. Measurements were performed in triplicates at room temperature (21 °C) in water.

To evaluate this approach, a 50 base ssRNA template was mixed with excess amount of complementary ssRNA of varying length (15, 30 and 45 bases) and annealing was carried out to achieve base-pairing. Measuring the fluorescence from these samples with SYBR Green I, SYBR Green II, and MeS **1** present, gave four measurement points for each dye-RNA combination, as shown in Figure 12. While neither of the SYBR Green dyes exhibited a linear dependence on RNA duplex, it was possible to construct a linear calibration curve for the MeS **1**. To further test this in practice, we attempted to determine the fraction of double-stranded RNA in released enterovirus EV1 RNA genome. As before, the virus opening was induced by adjusting the salt concentrations and increasing the temperature to 37 °C [28] allowing dyes to intercalate into the viral RNA. After preparing a calibration curve for MeS **1** in the capsid opening conditions, an EV1 sample containing equal amounts of RNA and dye (as applied to construct the calibration curve) was measured over the course of 180 minutes (Figure S29). From this, the highest attained emission value was compared to the calibration curve (Figure 13). This result corresponds to 51 % of the viral RNA is in duplex form, which supports previous estimations stating that the viral RNA is expected to have large secondary structures [29,30].

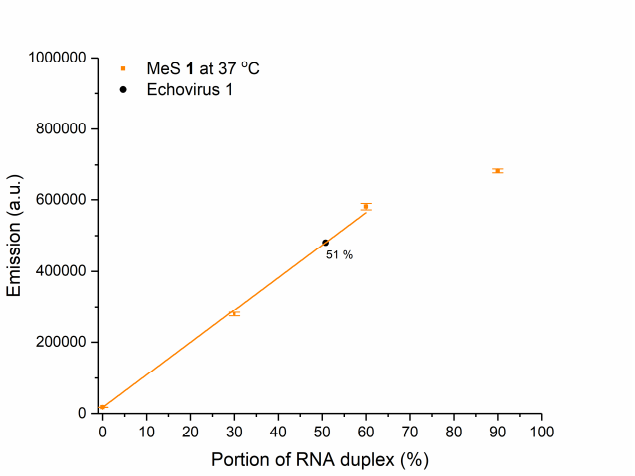

Figure 13. MeS **1** measured with partially double-stranded RNA oligomers. The emission value from a sample of EV1 containing equal concentration of RNA and MeS **1** (Figure S29) was inserted to the linear fit to yield the fraction of duplex RNA found in the sample. Measurements were performed in triplicates at 37 °C in 20 mM NaCl, 6 mM KH_2PO_4, 12 mM K_2HPO_4.

As an effect of the increased temperature and/or salt concentrations, the linearity of the calibration curve does not hold with the 45-mer sample, which underlines the importance of careful parametrization of the experiment for achieving reliable results throughout the full range of duplex formation. By increasing the amount of MeS **1** in experiments, the overall emission intensity can be increased to higher values compared to those attainable with SYBR Green II. Additionally, MeS **1** dye is more accommodating in this regard, because of its combined binding site size requirement and affinity for nucleic acid binding, as described in the previous section. Admittedly, similar results

could be achieved with SYBR Green I and SYBR Green II, but the lower binding affinity and binding site size make MeS **1** a more universal choice, due to increased ease in adjusting concentrations in the experiments to achieve linearity. With such a calibration curve, the single-to-double-stranded RNA ratio of an unknown sample of equal mass of RNA can be determined. In this work, viral RNA of EV1 was used as an example Information regarding the state of secondary structure of ssRNA should provide useful information for the continuously increasing number of studies on RNA.

In conclusion, the two newly synthesized dyes MeS **1** and NHS **4** expand the potential of nucleic acid sensing with SYBR Green related cyanine dyes in two very different ways. While MeS **1** can be used to increase fluorescence emission intensity with RNA samples, its linear response to changes in portion of double-stranded RNA offers an enhanced application as shown above. NHS **4** on the other hand offers new possibilities for better targeting, as shown above by covalently linking the dye on a viral capsid surface. Similar click chemistry can be applied to any primary amine group from antibodies to nanoparticles, opening countless possibilities for refined nucleic acid sensing.

3. Conclusion

The successful crystallization of SYBR Green II led to elucidation of the previously unknown structural characteristics of this well-established RNA marker. Knowledge of the structure of the indole-quinolinium-based cyanine dye enabled us to design a synthesis protocol to easily produce other 2-thiol substituted cyanine dyes at an analytical scale. This procedure was then employed to synthesize dyes **1**-**5** with varying 2-substituents, with the aim to add the potential of post-synthetic conjugation to *e.g.* antibodies or solid support.

The synthesized MeS **1** provides the highest fluorescence intensity when bound to nucleic acids and, importantly, higher in comparison to SYBR Green II, whereas compounds **2**-**5** gave lower values. Detailed studies between the synthesized and commercial dyes suggest that all the compounds are sensitive for nucleic acid sensing but MeS **1** as the smallest molecule takes less space in binding leading to higher overall emission compared to SYBR Green II. This is because the increasing size of the 2-substituent makes single molecules occupy more space on the nucleic acid strand and hence fewer molecules saturate the binding area available, leading to decreased fluorescence. These results offer fundamental understanding on the effects that different substituents might have on such intercalators. Regardless, all the synthesized dyes **1**-**5** exhibited considerable brightness.

Importantly, we could show with viral RNA samples that the produced dyes can sensitively detect RNA in biologically relevant assays. The dyes detected virus opening and RNA release *in vitro*: both unconjugated and a functionalized dye conjugated directly to viral particles detected virus opening in our developed real-time assay. This promises that the conjugated dyes in the future can be used to detect uncoating in cellular vesicles *in situ*. Similarly, the NHS-functionalized compound **4** can readily be employed for conjugation to any primary amine, providing added function for detection of nucleic acids with this class of fluorophores. Furthermore, the hydroxyl- and carboxylic acid functionalized dyes **2** and **3** can readily be employed to conjugate these dyes to a solid support or a biomolecule using carbodiimide crosslinking chemistry and thereby preventing dilution effects such as diffusion through cell membranes. Although the brightness of these dyes (**2**-**5**) is lower due to their longer 2-substituents, these functional groups offer the possibility of a localized, non-diffusing source of fluorescence, which can be an attractive option for various microscopy imaging applications.

4. Experimental Section

All reagents are commercially available and used as received unless otherwise mentioned. 1,2-dichloroethane (DCE) was distilled over $CaCl_2$ and stored under nitrogen over 3 Å molecular sieves. K_2CO_3 was dried in an oven at 120 °C and stored in a desiccator. SYBR Green I and II were purchased from Invitrogen as a solution in DMSO. Double-stranded bacterial plasmid λDNA (GLP-GPI 0.52 µg/µl) was received from ETH Zurich. Calf thymus (ct) DNA was purchased from Sigma-Aldrich. The 50 base long, single stranded DNAs were purchased from TAG Copenhagen A/S (Fredriksberg, Denmark) with sequences 5´-ACC AAA CTC AAC ACA CGA ACC CAA CGT TGG GTT CGT GTG TTG AGT TTG GT-3´ (hairpin DNA, hpDNA) and 5´-ACC CAC ACA ACC ACA AAC CAC ACC CAA CCC AAA CCC ACA CAC CCA ACA AC-3´ (linear DNA, liDNA) designed to promote hairpin and linear conformation of the oligomers, respectively. Both oligomers were dissolved in ddH_2O and the hpDNA was heated in boiling water bath for 3 minutes and allowed to cool down prior to use. Single stranded RNA oligomers were purchased from Eurofins Genomics (Ebersberg, Germany) as a 50 base template with sequence 5´-CCC AAC ACA ACC ACC AAC CAC AAA CAA CCC AAA CCC ACA CCA ACA ACA AAC-3´ and three complementary U/G strands of 15, 30 and 45 bases in length from the 3´ end (5´-UGU UGG UGU GGG UUU GGG UUG UUU GUG GUU GGU GGU UGU GUU GGG-3´). Cellular RNA (rRNA), was harvested from adenocarcinomic human alveolar basal epithelial cells (A549). The extraction was conducted using High Pure Viral RNA kit from Roche (Indianapolis, USA) following the instructions provided by the manufacturer. The concentration and purity of the extracted RNA was measured using Thermo Scientific NanoDrop One UV-vis spectrophotometer.

^{1}H, ^{13}C and 2D NMR (HSQC and HMBC) spectra were recorded with Bruker Avance 500 MHz and Bruker Avance 300 MHz spectrometers and chemical shifts were calibrated to the residual proton or carbon resonance of the solvent. Accurate HRMS spectra were measured with Micromass LCT ESI-TOF mass spectrometer using Leucine Enkephalin as the internal calibration. Atomic coordinates and structure factors for the reported crystal structures have been deposited with the Cambridge Crystallographic Data Centre (CCDC) under accession numbers 1482404 (SYBR Green II) and 1482405 (MeS **1**).

For comprehensive synthetic and experimental details please see the Supporting Information.

Acknowledgements

This work was supported by the Academy of Finland [266492 to T.-R.T and V.S., and 257125 to V.M.]; Jane & Aatos Erkko Foundation [Novel probes for discovering anti-virals to V.S., T.L., and V.M.]; and the Swedish Foundation for Strategic Research [IRC15-0065 for J.R.N., and L.M.W.]. GLP-GPI plasmid was obtained as a kind gift from Lucas Pelkmans from ETH Zurich.

Keywords: cyanines • nucleic acids • fluorescent probes • RNA recognition • host-guest systems • viruses

[1] Bruce A. Armitage. Cyanine Dye–Nucleic Acid Interactions. In: Strekowski L, editor. Top. Heterocycl. Chem. 14th ed., Pittsburgh: Springer; 2008, p. 11–29. https://doi.org/10.1007/7081_2007_109.

[2] Mojzych M, Maged H. Synthesis of Cyanine Dyes. Top. Heterocycl. Chem., Springer; 2008, p. 1–9.

[3] Shindy HA. Fundamentals in the chemistry of cyanine dyes: A review. Dye Pigment 2017;145:505–13. https://doi.org/10.1016/j.dyepig.2017.06.029.

[4] Choyke PL, Alford R, Simpson HM, Duberman J, Craig Hill G, Ogawa M, et al. Toxicity of organic fluorophores used in molecular imaging: Literature review. Mol Imaging 2009;8:341–54. https://doi.org/10.2310/7290.2009.00031.

[5] Lee LG, Chen C, Chiu LA. Thiazole orange: A new dye for reticulocyte analysis. Cytometry 1986;7:508–17. https://doi.org/10.1002/cyto.990070603.

[6] Vasilev AA, Kandinska MI, Stoyanov SS, Yordanova SB, Sucunza D, Vaquero JJ, et al. Halogen-containing thiazole orange analogues - New fluorogenic DNA stains. Beilstein J Org Chem 2017;13:2902–14. https://doi.org/10.3762/bjoc.13.283.

[7] Guo RJ, Yan JW, Chen S Bin, Gu LQ, Huang ZS, Tan JH. A simple structural modification to thiazole orange to improve the selective detection of G-quadruplexes. Dye Pigment 2016;126:76–85. https://doi.org/10.1016/j.dyepig.2015.11.010.

[8] Karlsson HJ, Bergqvist MH, Lincoln P, Westman G. Syntheses and DNA-binding studies of a series of unsymmetrical cyanine dyes: Structural influence on the degree of minor groove binding to natural DNA. Bioorganic Med Chem 2004;12:2369–84. https://doi.org/10.1016/j.bmc.2004.02.006.

[9] Deligeorgiev TG, Gadjev NI, Vasilev AA, Maximova VA, Timcheva II, Katerinopoulos HE, et al. Synthesis and properties of novel asymmetric monomethine cyanine dyes as non-covalent labels for nucleic acids. Dye Pigment 2007;75:466–73. https://doi.org/10.1016/j.dyepig.2006.06.023.

[10] Shank NI, Pham HH, Waggoner AS, Armitage BA. Twisted cyanines: A non-planar fluorogenic dye with superior photostability and its use in a protein-based fluoromodule. J Am Chem Soc 2013;135:242–51. https://doi.org/10.1021/ja308629w.

[11] Invitrogen. The Molecular Probes Handbook: A Guide to Fluorescent Probes and Labeling Technologies. Life Technologies Corporation; 2010.

[12] Zipper H, Brunner H, Bernhagen J, Vitzthum F. Investigations on DNA intercalation and surface binding by SYBR Green I, its structure determination and methodological implications. Nucleic Acids Res 2004;32:e103. https://doi.org/10.1093/nar/gnh101.

[13] Evenson WE, Boden LM, Muzikar KA, Oleary DJ. 1H and 13C NMR assignments for the cyanine dyes SYBR safe and thiazole orange. J Org Chem 2012;77:10967–71. https://doi.org/10.1021/jo3021659.

[14] Ihmels H, Otto D. Intercalation of Organic dye molecules into double-stranded DNA - General principles and recent developments. Top Curr Chem 2005;258:161–204. https://doi.org/10.1007/b135804.

[15] Karunakaran V, Pérez Lustres JL, Zhao L, Ernsting NP, Seitz O. Large dynamic stokes shift of DNA intercalation dye Thiazole Orange has contribution from a high-frequency mode. J Am Chem Soc 2006;128:2954–62. https://doi.org/10.1021/ja056862n.

[16] Dragan AI, Casas-Finet JR, Bishop ES, Strouse RJ, Schenerman MA, Geddes CD. Characterization of PicoGreen interaction with dsDNA and the origin of its fluorescence enhancement upon binding. Biophys J 2010;99:3010–9. https://doi.org/10.1016/j.bpj.2010.09.012.

[17] Geddes CD, Dragan AI, Casas-Finet JR, Schenerman MA, McGivney JB, Strouse RJ, et al. SYBR Green I: Fluorescence Properties and Interaction with DNA. J Fluoresc 2012;22:1189–99. https://doi.org/10.1007/s10895-012-1059-8.

[18] Fei X, Gu Y. Progress in modifications and applications of fluorescent dye probe. Prog Nat Sci 2009;19:1–7. https://doi.org/10.1016/j.pnsc.2008.06.004.

[19] Jin X, Yue S, Singer VL, Jones LJ, Beaudet MP, Cheung C-Y, et al. Characterization of SYBR Gold Nucleic Acid Gel Stain: A Dye Optimized for Use with 300-nm Ultraviolet Transilluminators. Anal Biochem 2003;288:278–88. https://doi.org/10.1006/abio.1998.3067.

[20] Crnolatac I, Rogan I, Majić B, Tomić S, Deligeorgiev T, Horvat G, et al. Small molecule probes finely differentiate between various ds- and ss-DNA and RNA by fluorescence, CD and NMR response. Anal Chim Acta 2016;940:128–35. https://doi.org/10.1016/j.aca.2016.08.021.

[21] Das AK, Ihmels H, Kölsch S. Diphenylaminostyryl-substituted quinolizinium derivatives as fluorescent light-up probes for duplex and quadruplex DNA. Photochem Photobiol Sci 2019;18:1373–81. https://doi.org/10.1039/c9pp00096h.

[22] Ying L. Nucleic acid detections and methods of their use. 2013/0137875, 2013.

[23] Neises B, Steglich W. Simple Method for the Esterification of Carboxylic Acids. Angew Chemie - Int Ed 1978;17:522–4.

[24] McGhee JD, von Hippel PH. Theoretical aspects of DNA-protein interactions: Co-operative and non-co-operative binding of large ligands to a one-dimensional homogeneous lattice. J Mol Biol 1974;86:469–89. https://doi.org/10.1016/0022-2836(74)90031-X.

[25] Molecular Probes. SYBR ® Green II RNA Gel Stain Product Information Sheet. 2001:1–3.

[26] Invitrogen. SYBR ® Green I Nucleic Acid Gel Stain Product Information Sheet. 2006:1–5.

[27] Martikainen M, Salorinne K, Lahtinen T, Malola S, Permi P, Häkkinen H, et al. Hydrophobic pocket targeting probes for enteroviruses. Nanoscale 2015:17457–67. https://doi.org/10.1039/c5nr04139b.

[28] Ruokolainen V, Domanska A, Laajala M, Pelliccia M, Butcher SJ, Marjomäki V. Extracellular albumin and endosomal ions prime enterovirus particles for uncoating that can be prevented by fatty

acid saturation. J Virol 2019. https://doi.org/10.1128/jvi.00599-19.

[29] Simmonds P, Tuplin A, Evans DJ. Detection of genome-scale ordered RNA structure (GORS) in genomes of positive-stranded RNA viruses: Implications for virus-evolution and host persistence. Bioinformatics 2004;10:1337–51. https://doi.org/10.1261/rna.7640104.

[30] Davis M, Sagan SM, Pezacki JP, Evans DJ, Simmonds P. Bioinformatic and Physical Characterizations of Genome-Scale Ordered RNA Structure in Mammalian RNA Viruses. J Virol 2008;82:11824–36. https://doi.org/10.1128/jvi.01078-08.

[31] Cosa G, Focsaneanu KS, McLean JRN, Scaiano JC. Direct determination of single-to-double stranded DNA ratio in solution applying time-resolved fluorescence measurements of dye-DNA complexes. Chem Commun 2000;8:689–90. https://doi.org/10.1039/b000473l.

[32] Beach L, Schweitzer C, Scaiano JC. Direct determination of single-to-double stranded DNA ratio in solution using steady-state fluorescence measurements. Org Biomol Chem 2003;1:450–1. https://doi.org/10.1039/b209284k.

Highlights:

- Previously unknown structure of SYBR Green II RNA stain was unveiled.
- New cyanine dyes aimed for post-synthetic conjugation were synthesized.
- One of the dyes shows higher sensitivity to RNA compared to SYBR Green II.
- Dye was conjugated to viral capsid surface and RNA release was observed with it.
- Quantitative method to determine the amount of RNA duplex in a sample was developed.

Author Contributions

Writing: VS (leading), KS, JN, VM, TL, MW, VR (supporting)
Data curation: VS (leading), KS, VR, JN (equal), TRT (supporting)
Formal analysis: VS (leading), KS, JN, TRT, VR, TL, SO (supporting)
Investigation: VS (leading), KS, VR, JN, TL
Funding acquisition: VM, MW
Project administration: VM

Declaration of interests

☒ The authors declare that they have no known competing financial interests or personal relationships that could have appeared to influence the work reported in this paper.

☐The authors declare the following financial interests/personal relationships which may be considered as potential competing interests: